

Consequences of Preset Pitch Angle on Cross-Flow Turbine Hydrodynamics

Benjamin Strom

Dept. of Mechanical Engineering, University of Washington
Stevens Way, Box 352600, Seattle, WA, 98195, USA
strombw@uw.edu

Brian Polagye

Dept. of Mechanical Engineering, University of Washington
Stevens Way, Box 352600, Seattle, WA, 98195, USA
bpolagye@uw.edu

Steve Brunton

Dept. of Mechanical Engineering, University of Washington
Stevens Way, Box 352600, Seattle, WA, 98195, USA
sbrunton@uw.edu

Abstract—The energy conversion efficiency of a straight-bladed cross-flow turbine is examined experimentally. The preset pitch angle of the turbine blades is shown to have a large impact on turbine performance for two and four-bladed turbines over the range of tip-speed ratios tested. The optimal preset pitch angle was found to be 6° for both turbines and nearly all tip-speed ratios. The nominal (apparent) angle of attack in the foil frame of reference is shown to depend only on tip-speed ratio and preset pitch angle if induced velocities are neglected. Turbine performance trends are described via a critical nominal angle of attack, hypothesized to be important during dynamic stall of the foil. Interaction of the foil with a leading edge vortex generated during the dynamic stall process is proposed as an explanatory mechanism for other turbine performance trends. Other hydrodynamic factors possibly influencing turbine performance are discussed briefly.

Index Terms—Hydrokinetic Energy, Cross-Flow Turbine, Pitch Angle, Tip-Speed Ratio, Dynamic Stall, Vortex Dynamics

I. INTRODUCTION

The majority of tidal energy turbine installations and prototypes to date have been of the axial flow type [1]. Cross-flow turbines present several possible advantages for hydrokinetic energy conversion. First, their rectangular form factor is well suited to take advantage of the concentration of kinetic energy in shallow channels (tidal or fluvial). In addition they provide an opportunity to construct high-blockage-ratio arrays, potentially increasing the total energy capture significantly over an array of axial flow turbines [2]. Second, they are well suited to bidirectional operation such as in tidal applications as an active yaw mechanism is unnecessary. Third, the maximum blade speed of a cross-flow turbine is generally a fraction of that of an axial flow type turbine [1]. This reduces the risk of damage to the blades via cavitation, and potentially reduces the risk of negative environmental impacts via acoustic pollution or physical interaction with marine fauna. Finally, cross-flow turbines can be arranged such that multiple turbine units drive the same generator, potentially reducing total array expense.

The variation in flow conditions encountered by a single blade during a single rotation in a cross-flow turbine makes the hydrodynamics significantly more complex than in an axial

flow turbine. With the objective of maximizing energy conversion efficiency, here we explore the hydrodynamic effects of altering preset blade pitch angle and tip-speed ratio.

A. Cross-Flow Turbine Design and Operation Parameters

The parameters responsible for the energy conversion performance of a cross-flow turbine are given in tables I and II.

These parameters are then collapsed into the following non-dimensional parameters: Aspect ratio

$$AR = \frac{2R}{L}, \quad (1)$$

solidity

$$\sigma = \frac{Nc}{2\pi L}, \quad (2)$$

chord-to-radius ratio

$$R_c = \frac{c}{R}, \quad (3)$$

tip-speed ratio (TSR),

$$\lambda = \frac{\omega R}{U_\infty}, \quad (4)$$

TABLE I

TURBINE GEOMETRY PARAMETERS

R	Turbine radius
L	Turbine span (height)
c	Blade chord
N	Blade count
α_p	Preset blade pitch angle
β	Blade helix angle
-	Blade profile
-	Blade end condition

TABLE II

TURBINE OPERATION PARAMETERS

U_∞	Incoming freestream flow velocity
-	free-stream turbulence
ω	Turbine angular velocity
τ	Turbine torque
-	Generator conversion efficiency

and the optimization objective, conversion efficiency

$$C_p = \frac{\omega\tau}{\frac{1}{2}\rho U_\infty^3 2RL}, \quad (5)$$

where ρ is the fluid density.

The preset blade pitch is defined as the angle between foil centerline at the quarter chord and the line tangent to the turbine circumference (see Fig. 1). We define a positive angle in the aerodynamic sense: pitch-up relative to the nominal free-stream direction is positive.

B. Cross-Flow Turbine Hydrodynamics

The hydrodynamics of cross-flow turbines can be reduced to three semi-interdependent categories: induced flow, three dimensional effects (flow variation in the span-wise direction), and individual foil hydrodynamics. Induced flow includes axial and angular induction, internal wake deficit, and the generation of coherent structures. Three dimensional effects include the role of the blade end condition (free vs. end plates), the turbine aspect ratio, and the hydrodynamics of blades with a helical sweep. Individual foil hydrodynamics include the effect of the variation of the nominal angle of attack and velocity with azimuthal blade position. The focus of this paper is on the effect of the nominal angle of attack and interaction with induced coherent structures on turbine performance.

Tip-speed-ratio, preset pitch angle, free-stream velocity, and the self-induced velocity field are all responsible for the variation of the nominal angle of attack, α_n , with the azimuthal blade position, θ (Fig. 1). If we assume the turbine imparts no changes in flow velocity and hold the remainder of the responsible parameters constant throughout the blade rotation, the analytic expression for the instantaneous nominal angle of attack is given by

$$\alpha_n = \tan^{-1} \left(\frac{\omega R \sin(\alpha_p) + U_\infty \sin(\alpha_p - \theta)}{\omega R \cos(\alpha_p) + U_\infty \cos(\alpha_p - \theta)} \right), \quad (6)$$

or in terms of TSR, λ

$$\alpha_n = \tan^{-1} \left(\frac{\lambda \sin(\alpha_p) + \sin(\alpha_p - \theta)}{\lambda \cos(\alpha_p) + \cos(\alpha_p - \theta)} \right). \quad (7)$$

We see then that TSR and preset pitch angle are solely responsible for the azimuthal variation in nominal angle of attack. For various combinations of these parameters $\alpha_n(\theta)$ is given in Fig. 2. In general, increasing the TSR reduces the maximum nominal angle of attack. Increasing the preset pitch angle decreases the nominal angle of attack magnitude during the upstream portion of the blade cycle while increasing it during the downstream portion of the cycle.

The parameters used to generate Fig. 3 fall within the range of parameters tested experimentally. Thus, there is a potential for large nominal angles of attack during the cycle. This suggests that dynamic stall may occur, producing significant unsteady fluid forcing. If the maximum angle of attack is large enough, a leading edge vortex will be generated during the rotation [3], which may subsequently impart transient forces on the blade.

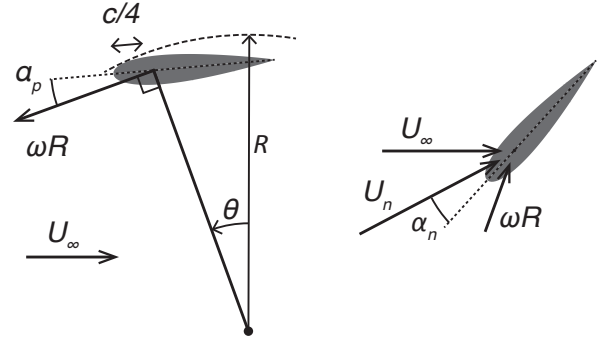


Fig. 1. Preset blade pitch, α_p (left) and nominal angle of attack, α_n (right). The azimuthal blade position is denoted by θ ($\theta = 0$ when $\omega \times R$ points directly upstream). The free-stream velocity is U_∞ and the nominal velocity U_n .

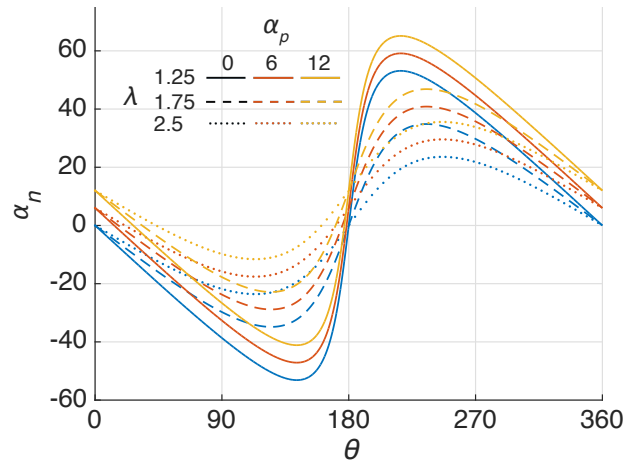


Fig. 2. The effect of preset blade pitch (α_p) on nominal angle of attack (at the mount point, $c/4$ from the leading edge) for various TSRs (λ). This assumes no induced flow velocity.

C. High Chord-to-Radius Turbines

Cross-flow turbines for wind power (referred to as vertical axis wind turbines) generally have a low chord-to-radius ratio, and thus a low solidity. However, for hydrokinetic applications, high chord-to-radius turbines present several advantages. Previous experiments show that the optimal TSR for vertical axis wind turbines is inversely related to the chord-to-radius ratio. The lower optimal TSR is advantageous for hydrokinetic applications due to a reduced risk of cavitation, decrease in structural vibration frequency and magnitude, and reduced risk to marine fauna. In addition, the larger relative chord length allows more structurally robust blades.

The high chord-to-radius ratio introduces another level of complexity to the hydrodynamics as the nominal angle of attack can vary significantly over the foil chord length (Fig. 3).

D. Prior Work

Klimas and Worstell (1981) tested preset pitch angles up to 7° experimentally on a vertical axis wind turbine, finding

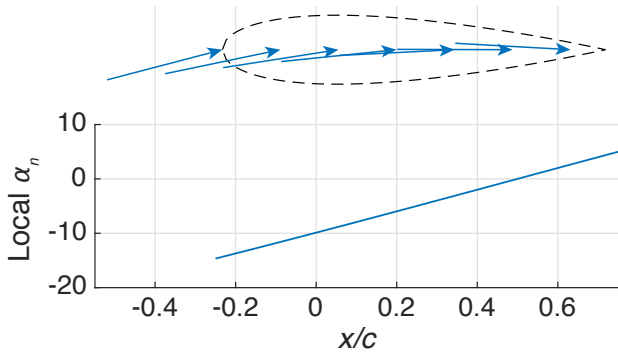


Fig. 3. Local nominal angle of attack variation along the chord length. Here $\theta = 30^\circ$, $\alpha_p = 0$, $\lambda = 2$, and $Re_c = 0.5$. $x = 0$ is at the mount point, $c/4$.

an optimal preset pitch of 2° [4]. Fieldler and Tullis (2009) tested three different preset pitch angles experimentally on a three bladed vertical axis wind turbine. They found a 29% increase in performance for a 7.8° preset pitch angle over the zero preset pitch angle case [5]. Two dimensional numerical simulations by McLaren, Tullis, and Ziada (2012) of a high solidity turbine illustrate the production of a single large leading edge vortex [6].

II. METHODS

Previous experiments suggest turbine performance is sensitive to chord-based Reynolds number. For this reason, as well as the difficulties in capturing the complex hydrodynamics outlined above, the parameter space is explored experimentally rather than numerically.

A. Flume

Experiments were performed in a water flume with a 75 cm x 48 cm deep (while running) test section. The blockage ratio (the ratio of the turbine swept area to the flume cross sectional area) was 0.11. Previous studies suggest blockage values over about 0.05 will inflate turbine performance measurements compared to performance in unconfined flow [7] [8]. The flume was run at a nominal velocity of 0.7 m/s. The free-stream velocity was measured concurrently with other measurements $10R$ upstream from the turbine using an acoustic Doppler velocimeter at a sample rate of 32 Hz. This point velocity measurement was centered on the turbine in the directions perpendicular to the free-stream velocity. The turbulent intensity of the incoming flow was 1.8%. The blade chord Reynolds number, given by

$$Re_c = \frac{U_\infty c}{\nu}, \quad (8)$$

was 3.2×10^4 . This simplified expression neglects both turbine angular velocity and induction. Inclusion of the angular velocity yields and azimuthal foil position dependence, given by

$$Re_c(\theta) = \frac{U_\infty [\lambda + \cos(\theta)] c}{\nu} \quad (9)$$

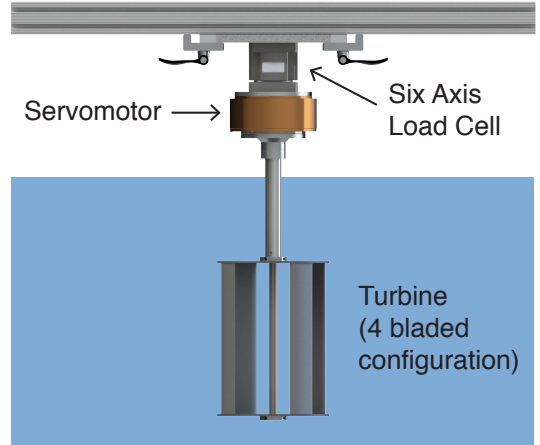


Fig. 4. Experimental setup. The free-stream velocity direction is into the page. The turbine was centered horizontally and vertically in the test section.

For these experiments, this results in a maximum Reynolds number of 6.3×10^4 for $\lambda = 1$ and 1.1×10^5 for $\lambda = 2.5$.

B. Experimental Turbine

The cross-flow turbine used in this study consisted of two circular endplates mounted on a 1.3 cm diameter shaft. Straight blades were chosen over helical ones in order to resolve the hydrodynamic forcing with respect to the azimuthal blade position. These were mounted at the periphery of the end plates at various preset pitch angles, such that the maximum turbine radius remained constant at 8.6 cm. Preset pitch angles from were considered from 0° to 12° in increments of 2° . A symmetric NACA0018 blade profile with a 4.05 cm chord was used. Two-bladed and four-bladed turbines were tested with respective solidities of $\sigma = 0.15$, and 0.3. The turbine aspect ratio was 1.36 and the chord-to-radius ratio was 0.47.

C. Turbine Performance Measurement

The turbine was mounted at one end to a face-mount servomotor via a 2.5 cm shaft. The servomotor was mounted in turn to a six-axis load cell. In this study, only the torque on the axis of the turbine rotation is considered. The servomotor was operated in constant velocity mode isolating fluid forcing on the turbine by eliminating torque due to angular acceleration. Turbine position was measured via the 10^6 count per revolution encoder internal to the servomotor. The TSR was adjusted by altering turbine angular velocity. TSRs were considered from 0.8 to 2.8 in increments of 0.1. At each TSR, 60 seconds of force and position data was recoded at 1000 samples per second. The resulting energy conversion efficiency of the turbine was calculated as given in equation 5.

D. Flow Visualization

Two-dimensional flow field visualization was performed for select test cases ($\alpha_p = 0^\circ, 6^\circ$, and 12° , $\lambda = 1.3$ and 1.8). A transparent bottom endplate was used on the bottom of the

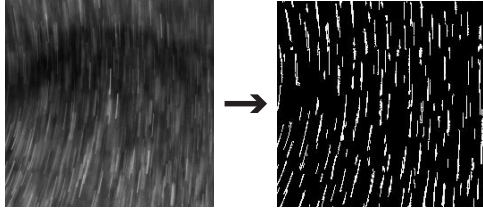


Fig. 5. A small section of bubble streak-lines from a high-speed video still (left) and after post-processing via localized thresholding and minimum contiguity (right).

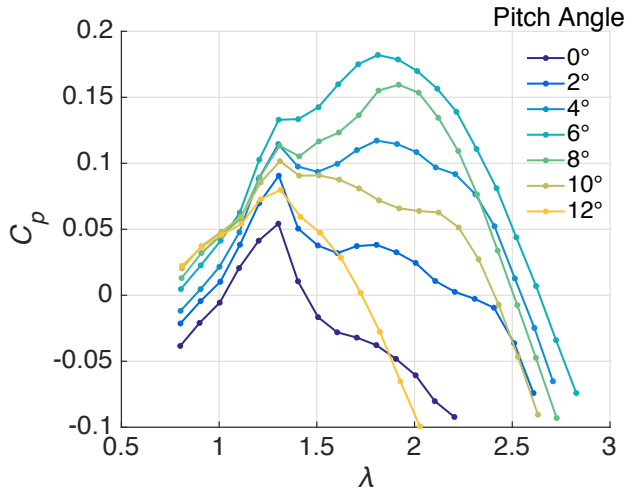


Fig. 6. Turbine coefficient of performance (C_p , or efficiency) vs TSR (λ) for various preset pitch angles for an $N = 2$ bladed turbine.

turbine. Bubbles of approximately $25\mu\text{m}$ in diameter were selectively illuminated with halogen lamps. A high speed camera positioned below the test section captured the motion of the bubbles at 200 frames per second at the mid-plane of the turbine, perpendicular to the axis of rotation. In order to provide streak-lines for a qualitative assessment of velocity magnitude and trajectory, the exposure time was set to 7 ms. This resulted in approximate streak-line length of 4.9 mm for the free-stream velocity of 0.7 m/s. The plane of inquiry was kept as thin as possible by increasing the aperture as much as allowable by the exposure time.

Post-processing of video frames was performed by localized thresholding in order to increase bubble visibility in blade shadows, followed by area opening via minimum connectivity (for de-speckling), the result of which is shown in Fig. 5.

III. RESULTS AND DISCUSSION

A. Performance Curves

Figures 6 and 7 show the turbine efficiency response with TSR for the two-bladed and four-bladed configurations respectively. We find turbine performance to be highly sensitive to preset pitch angle, with an optimum value of 6 degrees. The conversion efficiency increased from 5.4% with zero preset

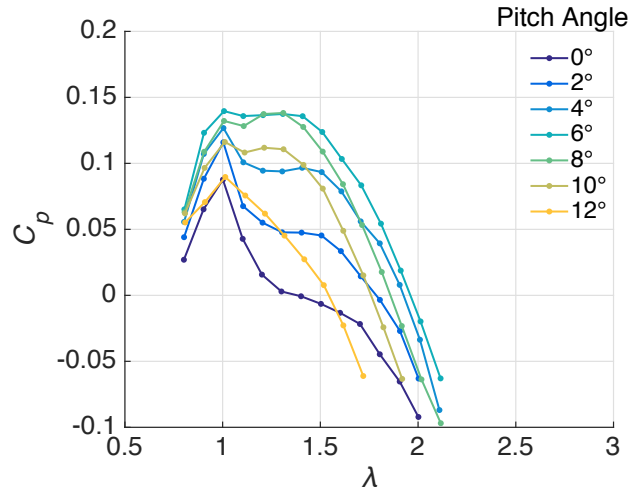


Fig. 7. Turbine coefficient of performance (C_p , or efficiency) vs TSR (λ) for various preset pitch angles for an $N = 4$ bladed turbine.

pitch angle to 18.2% at the optimum angle for the two-bladed case and from 8.8% to 14.0% for the four-bladed case.

A general explanation for the beneficial effect of increasing the preset pitch angle can be found by including the effect of the internal wake deficit in the calculation of the nominal angle of attack. The energy extracted from the flow by the blade during the upstream portion of the rotation results in a reduction in the free-stream velocity encountered by the blades during the downstream portion of the cycle. This reduces the magnitude of the nominal angle of attack for the downstream portion of the stroke. Increasing the pitch angle has the opposite effect, thus normalizing the maximum nominal angle of attack for the upstream and downstream portions of the stroke (see Fig. 8).

Though the maximum efficiency of the four-bladed turbine was significantly less that of the two-bladed turbine, performance was equivalent or better at TSRs less than or equal to one. Previous experiments indicate that a one-bladed turbine performs less well than a two-bladed turbine and with a higher optimal TSR. We hypothesize that the hydrodynamics responsible for an optimal number of blades is due to a balance of three factors. The addition of blades causes: Higher solidity and thus self blockage and flow diversion around the turbine, higher rotational drag per added bladed which reduces the optimal tip-speed ratio which in turn increases the maximum nominal angle of attack, and an increase in the frequency of fluid forcing per full turbine rotation.

For the remainder of the discussion, we focus on the factors that influence the performance of the two-bladed turbine. We propose that the behavior shown in Fig 6 can be partially explained via two hydrodynamic mechanisms: Lift and drag during the dynamic stall process for the upstream portion of the blade rotation, and the interaction of the foil with the resulting leading edge vortex.

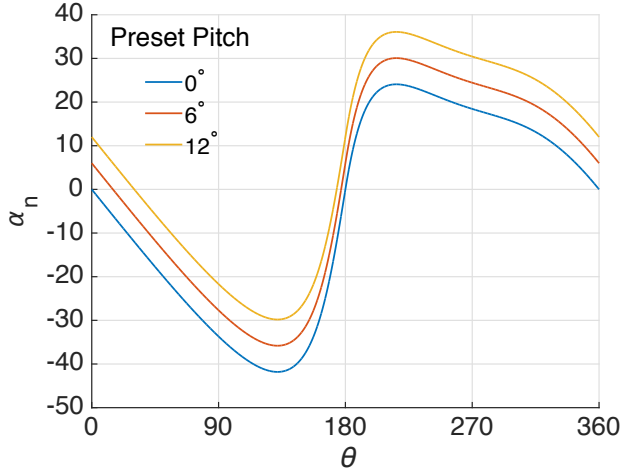


Fig. 8. The effect of preset pitch angle on nominal angle of attack via equation 7. This assumes a negative cosine induced velocity in the stream-wise direction with a minimum value of $0.5U_\infty$.

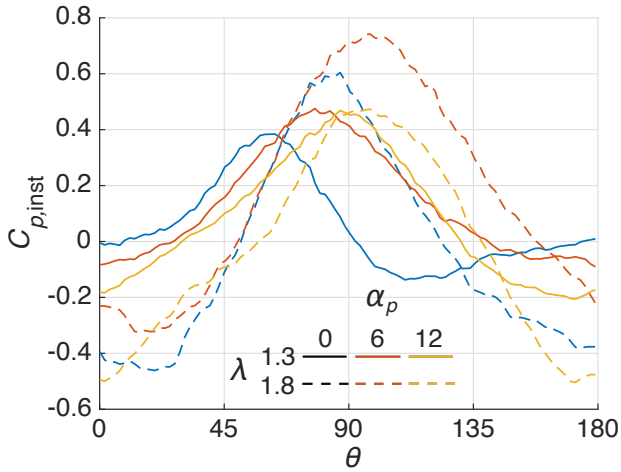


Fig. 9. Phase-averaged instantaneous efficiency for a two-bladed turbine at various TSRs and preset pitch angles. Only a half rotation is shown as this is the forcing period.

B. Instantaneous Power Profiles

For a constant angular rotation speed and free-stream flow velocity, the instantaneous conversion efficiency is solely a function of the torque due to the blade hydrodynamics. Figure 9 shows the phase-averaged power over half of a turbine rotation (the forcing period for a two-bladed turbine) for several TSR and preset pitch angle configurations. With a 60 second sample period and 100 bins per half revolution, we have an average of 600 sample points per bin. Due to the downstream wake deficit, the remainder of this analysis assumes that the positive power output portion of the stroke is dominated by the upstream blade hydrodynamics.

C. Dynamic Stall

The large range of the nominal angle of attack experienced by the foil throughout the rotation indicates that the foil undergoes dynamic stall [9]. Dynamic stall is characterized

by a transient increase in both the lift and drag forces during an increase in angle of attack well above their static values. The flow around the airfoil remains temporarily attached for higher angles than would normally be attached in the static case. The flow eventually separates, often leading to roll-up of the resulting shear layer into a vortex near the leading edge, which is referred to as the leading edge vortex (LEV) [3].

During the dynamic stall process, before and up to separation, the lifting force increases approximately linearly with increasing angle of attack [3]. The increase in the drag force over the static value is delayed and more abrupt than the lift force. As the lift force is beneficial to the power output of the turbine and the drag force is detrimental, at some critical angle of attack (α_{crit}), the benefit from the increase in lift force will be start to be overcome by the negative effect of the spike in drag force. If we assume that the majority of the power is due to the upstream blade, we can then hypothesize that the peak of the instantaneous power curve occurs at this critical nominal angle of attack. To test this, the peak of each instantaneous power curve is located with respect to the azimuthal blade position. Then equation 7 is used to calculate the nominal angle of attack at this location. The result is plotted in Fig. 10. The predicted critical angle of attack is quite consistent when the virtual pitching rate of the foil $\dot{\alpha}_n$ is rapid, and it is slightly less consistent during slower angular rates. However, no clear dependence on $\dot{\alpha}_n$ is observed, though it is considered important in many dynamic stall models [9].

Examination of the flow-field via bubble visualization shows that this critical nominal angle of attack corresponds to the onset of full separation. Figure 11 shows the flow field at the critical nominal angle of attack (left) and shortly afterwards (right) for two preset pitch angles. Though the azimuthal angle differs for the critical nominal angle of attack in each case (top vs. bottom), we see that in each case the leading edge vortex occurs shortly after the critical nominal angle, indicating that the critical angle of attack corresponds to the same location in the dynamic stall process.

The dynamic stall is dictated by the nominal angle of attack, which in turn is governed by the TSR and preset pitch angle. As such, we observe that dynamic stall is likely responsible for the rightward shift of the instantaneous power curves with increasing preset pitch angle and increasing TSR (Fig. 9). This is because both parameters delay or reduce the nominal angle of attack, thus delaying the azimuthal angle at which α_{crit} is reached. The possible exception to these trends in Fig. 9 is the $\lambda = 1.8$ and $\alpha_p = 12^\circ$ case. Equation 7 predicts that the nominal angle of attack never reaches the critical value for this parameter set. This observation is reinforced by flow visualization as the rollup of a LEV is not observed for this case.

We suggest that combinations of TSR and preset pitch angle that result in optimal turbine performance will maximize the lift associated with dynamic stall while minimizing the drag penalty due to total separation. To do so, the nominal angle of attack should reach the critical angle and no further. Figure 12 shows the absolute difference of the maximum nominal

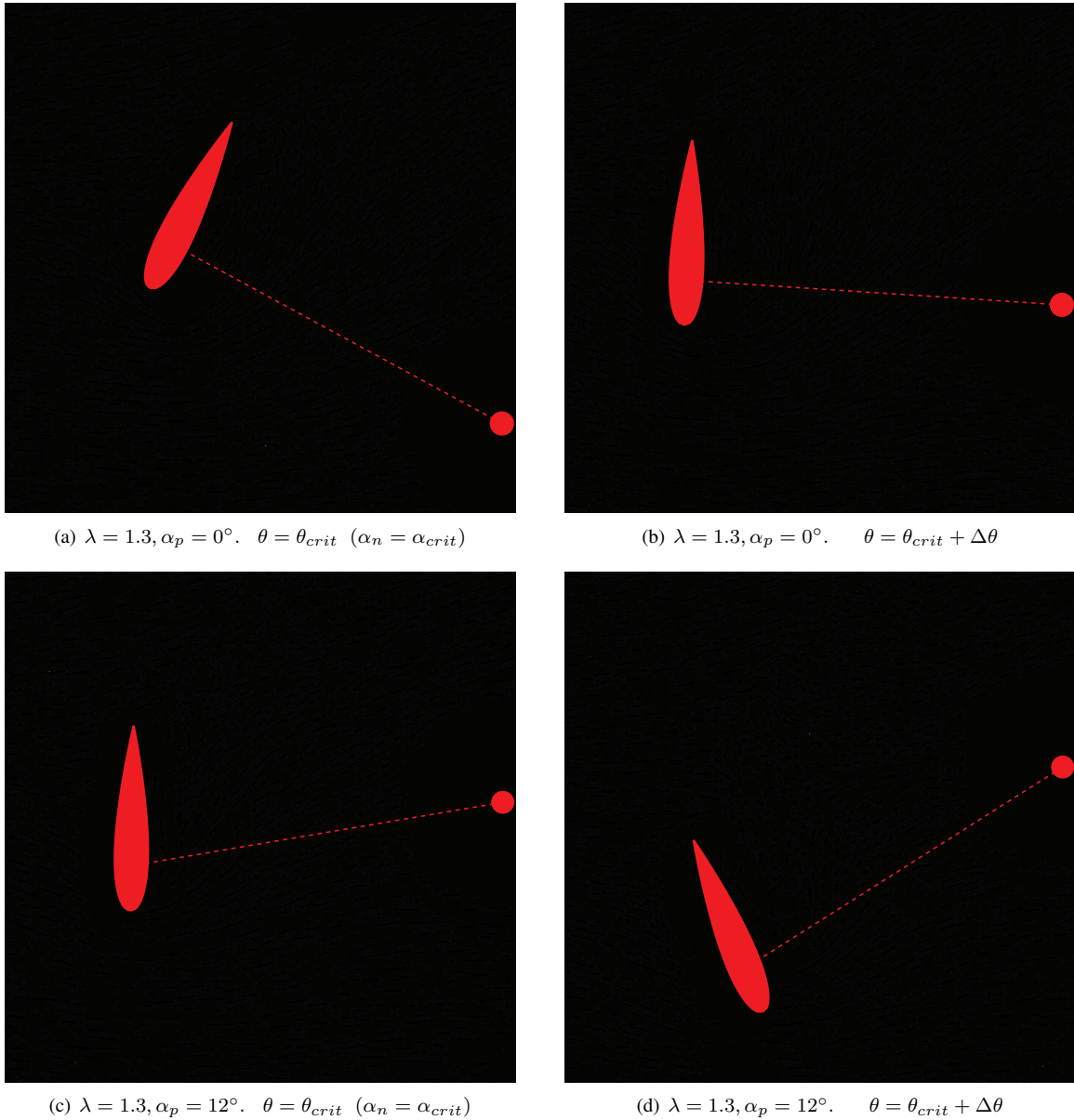


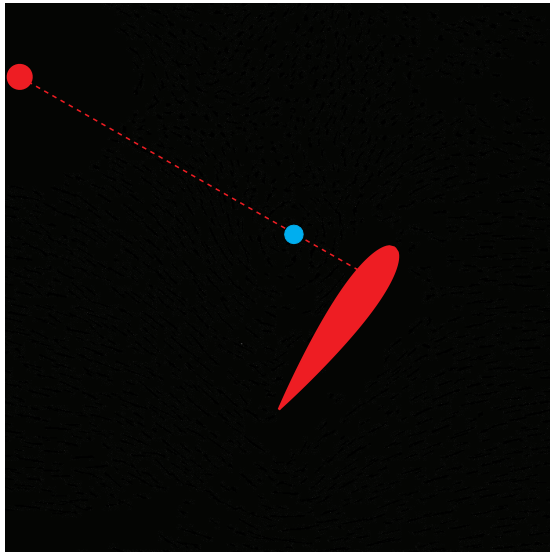
Fig. 11. Flow visualization via high-speed video of entrained bubbles with the blade position superimposed. The free-stream flows from left to right. The left images show the flow-field for the azimuthal position at which the critical nominal angle of attack (α_{crit}) is predicted to occur. The left images show the same flow-fields 15 ms later ($\approx 17^\circ$ of rotation at this TSR). The top and bottom sets are for 0° and 12° preset pitch angles respectively. Note that though the azimuthal angle differs between the two cases, the stage of dynamic stall is the similar, supporting the concept of a critical nominal angle of attack.

angle of attack and the critical angle. We see that our best performing case ($\lambda = 1.6, \alpha_p = 6^\circ$) minimizes this value, as predicted by our hypothesis. In fact, the location of this minimum predicts second peak (where $\lambda > 1.3$) in the performance curves for each preset pitch angle reasonably well. However, this method predicts good performance for some TSR- α_p combinations (such as $\lambda = 1.6, \alpha_p = 12^\circ$) which perform poorly. In addition, dynamic stall does not explain the peak in the performance curves for all preset pitch angles at $\lambda = 1.3$. This suggests additional criteria help dictate turbine performance.

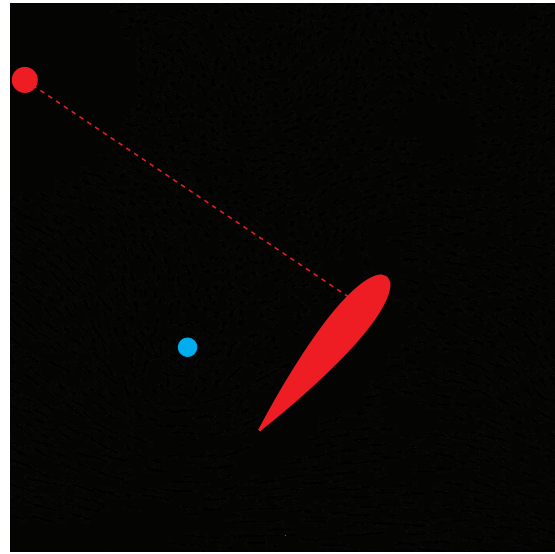
D. LEV-Foil Interaction

Flow-field visualizations show that the LEV vortex dynamics are dependent on the TSR. For TSRs of $\lambda > 1.3$, the downstream translation rate of the LEV is slower than the foil translation speed. As a result, the LEV translates towards the trailing edge of the foil, and is finally left behind completely. For TSRs of $\lambda \leq 1.3$, the LEV remains with the foil (at the leading edge). One example of this is shown in the flow visualizations in Fig. 13.

Previous studies show that the LEV is a low pressure region which exerts a suction force on the foil [9]. The effect of this is twofold: First, it causes the LEV to have a tendency to



(a) $\lambda = 1.3, \alpha_p = 6^\circ$



(b) $\lambda = 1.8, \alpha_p = 6^\circ$

Fig. 13. LEV location (highlighted by blue dot) well after formation for two TSRs, all other parameters held constant.

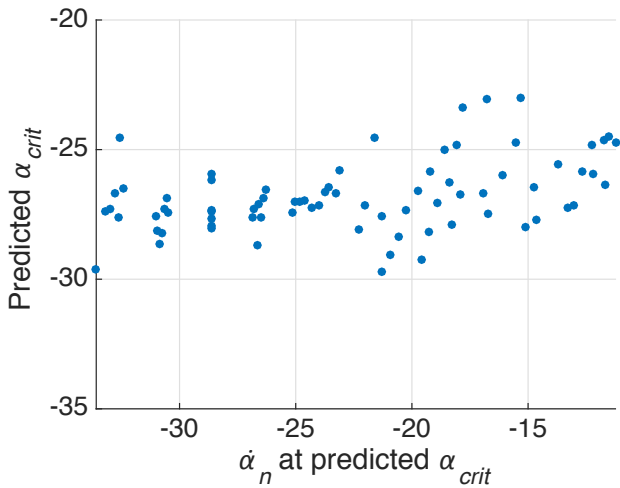


Fig. 10. Critical angle of attack predictions using the peak of the instantaneous power curves and the nominal angle of attack equation (7) for the test cases shown in Fig. 6. Cases where the nominal angle of attack never falls below -25° are omitted as it is likely these cases never reach the critical angle.

be “stuck” to the foil. This is why the LEV translates with the foil even if the foil is moving slightly faster or slower than the surrounding flow. This could be why we see an associated critical TSR greater than one. Second, it imparts a hydrodynamic force on the foil, which in turn impacts turbine performance. At $\lambda > 1.3$, this means the eventual location of the LEV near the trailing edge of the foil will result in a detrimental drag force. The influence of the LEV can be seen in the instantaneous efficiency curves in Fig. 9. The $\lambda = 1.3$ cases show a higher instantaneous efficiency for the azimuthal angles where the LEV is present (after the peak associated with the power from dynamic stall). The lift benefit from the LEV for these cases is offset by the fact that the opposing

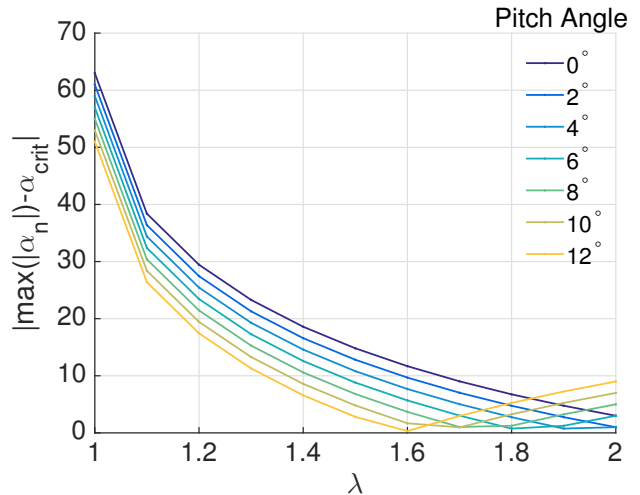


Fig. 12. The difference between the maximum nominal effective angle of attack magnitude and the predicted critical angle vs TSR at each preset pitch angle tested. We hypothesize that minimizing this value maximizes power production by halting the dynamic stall process where the benefit due to the transient lift force is overcome by the detrimental spike in drag force.

blade on the other side of the turbine is translating directly upstream during this portion of the cycle. The $\lambda = 1.8$ cases show a sharp decrease in efficiency during the same region, associated with the drag force, which is at least due to the lack of the lifting force from the well positioned LEV, and possible due to added drag associated with the vortex being located near the trailing edge.

In the high TSR regime ($\lambda > 1.3$), decreasing the preset pitch angle increases the maximum nominal angle of attack, likely increasing the strength of the LEV. This results in a larger drag force once the LEV translates toward the trailing edge of the foil, decreasing overall performance. A large preset

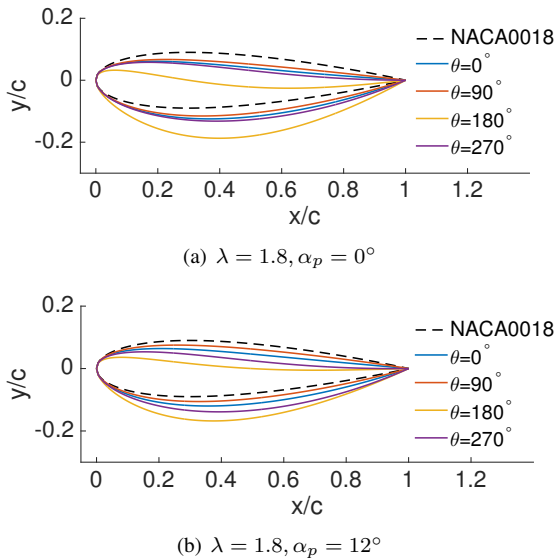


Fig. 14. Virtual induced camber as a function of azimuthal blade position for $\alpha_p = 0^\circ$ (top) and 12° (bottom). Maximum camber decreases with increased preset pitch angle.

pitch angle, though potentially eliminating the LEV altogether due to the small maximum nominal angle of attack, may never reach α_{crit} , thus failing to take full advantage of the dynamic stall as discussed previously.

E. Other Hydrodynamic Factors

Though dynamic stall and the resulting LEV-foil interaction appear to describe much of turbine performance response with changing TSR and preset pitch angle, several other factors may influence performance significantly. These are outlined below.

1) *Nominal Velocity*: As well as altering the nominal angle of attack, the TSR effects the magnitude of the nominal velocity experienced by the foil through the turbine rotation. This could explain the poor performance of some of the cases which otherwise undergo an optimal dynamic stall trajectory (those that are minimized in Fig. 12). If the TSR is not high enough, the low nominal velocity may result in lower forces, reducing power output.

2) *Virtual Foil Camber*: As depicted in Fig. 3, the nominal angle of attack can change significantly over the chord length of the foil. The hydrodynamic effect of the varying angle of attack (due to curvilinear flow) is analogous to a cambered airfoil in rectilinear flow [10]. Performing a remapping of the curvilinear flow, as given in [10], shows the analogous camber. As the nominal angle of attack depends on the TSR and preset pitch angle, so will the virtual camber. Figure 14 shows that increasing the preset pitch angle reduces the maximum camber of the foil. Moderate virtual camber could increase lift during favorable nominal angles of attack, though excessive virtual camber could increase drag during other portions of the cycle.

3) *Induced Velocity*: The effect of the extraction of energy from the free-stream flow by the blades during the upstream portion of the cycle on the resulting flow field experienced during the down stream portion remains unexplored (with the

exception of the LEV dynamics). This could affect power generation during the downstream portion of the cycle as well as drag on the foil as it translate upstream.

IV. CONCLUSION

Through experiments in a water flume, we find the energy conversion performance of a cross flow turbine to be highly sensitive to the preset blade pitch angle. For a two-bladed turbine, a 237% increase in performance was measured between the zero preset pitch angle case and the optimal preset pitch angle of six degrees. The corresponding increase for a four-bladed was 59%.

Two major factors influencing performance are identified: Dynamic stall and LEV-foil interaction. A critical nominal angle of attack associated with fluid forcing during dynamic stall is identified using the peak phase averaged instantaneous efficiency and an expression for the nominal angle of attack. This critical angle is found to be consistent across the parameter space. TSR and preset pitch angle combinations resulting in the highest turbine performance are those for which the maximum nominal angle of attack matches the critical value. A secondary peak in the two-bladed turbine performance curve at TSR of $\lambda = 1.3$ is shown to correspond to the point at which LEV translation speed matches the foil translation rate. As a result, the LEV remains near the leading edge, enhancing instantaneous power as the foil translates downstream.

Potential areas of future work include the quantitative analysis of the LEV formation and dynamics through particle image velocimetry, exploration of the factors that influence the induced velocity within the turbine and the resulting hydrodynamics, the effect of the varying nominal velocity magnitude with azimuthal blade position, and the potential influence of virtual foil camber on turbine performance.

ACKNOWLEDGMENT

We would like to thank Naval Facilities Engineering Command for funding this research.

Thanks are also given to the University of Washington's Department of Aeronautics and Astronautics and Fiona Spencer for use of their water flume, as well as to Prof. Alberto Aliseda for the loan of a high-speed camera.

REFERENCES

- [1] M. Khan, G. Bhuyan, M. Iqbal, and J. Quaicoe, "Hydrokinetic energy conversion systems and assessment of horizontal and vertical axis turbines for river and tidal applications: A technology status review," *Applied Energy*, vol. 86, no. 10, pp. 1823–1835, 2009.
- [2] S. Salter, "Are nearly all tidal stream turbine designs wrong?" in *4th International Conference on Ocean Energy*, 2012.
- [3] W. McCroskey, "The phenomenon of dynamic stall." National Aeronautics and Space Administration Moffett Field CA, AMES Research Center, Tech. Rep., 1981.
- [4] P. C. Klimas and M. H. Worstell, *Effects of blade preset pitch/offset on curved-blade Darrieus vertical axis wind turbine performance*. Sandia National Laboratories, 1981.
- [5] A. J. Fiedler and S. Tullis, "Blade offset and pitch effects on a high solidity vertical axis wind turbine," *Wind engineering*, vol. 33, no. 3, pp. 237–246, 2009.
- [6] K. McLaren, S. Tullis, and S. Ziada, "Computational fluid dynamics simulation of the aerodynamics of a high solidity, small-scale vertical axis wind turbine," *Wind Energy*, vol. 15, no. 3, pp. 349–361, 2012.

- [7] C. A. Consul, R. H. Willden, and S. C. McIntosh, "Blockage effects on the hydrodynamic performance of a marine cross-flow turbine," *Philosophical Transactions of the Royal Society A: Mathematical, Physical and Engineering Sciences*, vol. 371, no. 1985, p. 20120299, 2013.
- [8] A. L. Niblick, "Experimental and analytical study of helical cross-flow turbines for a tidal micropower generation system," Master's thesis, University of Washington, 2012.
- [9] T. C. Corke and F. O. Thomas, "Dynamic stall in pitching airfoils: Aerodynamic damping and compressibility effects," *Annual Review of Fluid Mechanics*, vol. 47, pp. 479–505, 2015.
- [10] P. Migliore, W. Wolfe, and J. Fanucci, "Flow curvature effects on darrieus turbine blade aerodynamics," *Journal of Energy*, vol. 4, no. 2, pp. 49–55, 1980.